The Fate of Cannibalized Fundamental-plane Ellipticals

The fate of cannibalized fundamental-plane ellipticals

Martin D. Weinberg[1]
Department of Physics and Astronomy
University of Massachusetts, Amherst, MA 01003-4525
weinberg@phast.umass.edu

ABSTRACT

Evolution and disruption of galaxies orbiting in the gravitational field of a larger cluster galaxy are driven by three coupled mechanisms: 1) the heating due to its time dependent motion in the primary; 2) mass loss due to the tidal strain field; and 3) orbital decay. Previous work demonstrated that tidal heating is effective well inside the impulse approximation limit. Not only does the overall energy increase over previous predictions, but the work is done deep inside the secondary galaxy, e.g. at or inside the half mass radius in most cases. Here, these ideas applied to cannibalization of elliptical galaxies with fundamental-plane parameters.

In summary, satellites which can fall to the center of a cluster giant by dynamical friction are evaporated by internal heating by the time they reach the center. This suggests that true merger-produced multiple nuclei giants should be rare. Specifically, secondaries with mass ratios as small as 1% on any initial orbit evaporate and those on eccentric orbits with mass ratios as small as 0.1% evolve significantly and nearly evaporate in a galaxian age. Captured satellites with mass ratios smaller than roughly 1% have insufficient time to decay to the center. After many accretion events, the model predicts that the merged system has a profile similar to that of the original primary with a weak increase in concentration.

Subject headings: stellar dynamics — galaxies: kinematics and dynamics — galaxies: evolution — galaxies: clusters — galaxies: nuclei — galaxies: elliptical

---

[1]Alfred P. Sloan Foundation Fellow.

1. Introduction

The current picture galaxy evolution in clusters leads naturally to galactic cannibalism, especially deep in the potential well where the giants reside. Although multiple nuclei candidates have been identified (e.g. Tonry 1985, Lauer 1988), recent searches turned up many fewer inner core objects than expected (Tremaine 1995).

A closer look at the evolutionary picture is motivated by the recent demonstration that heating of galaxies or star clusters due the time-dependent tidal field can drive their evolution at a rate beyond impulse approximation estimates (Weinberg 1994abc, hereafter W1–3 , Murali & Weinberg 1996ab, hereafter MW1–2). This theory invalidates the following often-used argument. The higher density of satellite galaxies implies shorter internal orbital times than the orbit of the satellite itself. Therefore, the stellar orbits in the satellite will adiabatically invariant to the tidal force, and since the dynamical friction time scale is much less than a Hubble time for galaxy masses above $10^9\,\mathrm{M}_\odot$, the satellite should sink to the center without suffering tidal disruption and remain a distinct compact entity. This paper presents estimates of the evolutionary path and evaporation lifetime for the cannibalized fundamental-plane elliptical galaxies. We will find that ellipticals with sufficient mass to decay are heated and evaporated before a multiple nucleus system can result, although such systems may exist transiently. The results also illustrate the interplay between tidal heating, tidal stripping and orbital decay. The likely evaporation of accreted galaxies may help reconcile the observation of a bimodal velocity distribution of multiple nuclei (Tonry 1985) as 1) a dynamical friction mediated selection effect (Merritt 1984) or recently captured secondary and 2) a transient population of evaporating secondaries.

We begin with a description of the astronomical scenario in §2. All members of the fundamental plane are represented by a spherical model with fixed concentration; this is consistent with the observed fundamental plane relations given the Faber-Jackson (1976) relation although the best estimates suggest a weak dependence on concentration. We assume that the secondary is captured from the cluster by dynamical drag and consider evolution after the secondary is bound to the primary. The important dynamical ingredients and their implementation is briefly discussed in §3; the technical details can be found in the Appendix and elsewhere (W2, MW2). The results for a number astronomical scenarios are described in §4; these include the survival and evolution as a function of mass, orbital decay, and the resulting distribution of stripped stars in the primary. A summary and discussion is presented in §5.

2. Astronomical scenario

2.1. Background profile and fundamental plane scaling

I have chosen a King model for both the primary and secondary. King models with $\log c = 2.35$ are representative elliptical profiles (e.g. Mihalas & Binney 1981, Vader & Chaboyer 1994) although King models are not good fits in all cases[2]. Nonetheless, the mass model parameterizes the range of stellar orbital times, and this range determines the overall evolution rate from the resonant heating process to be described below. An appropriate concentration ensures that a realistic range of orbital time scales are included. The conclusions (§4) are weakly dependent on the inner profile and other fine details of the model.

The radius and mass concentration chosen according to two fundamental plane relations. The first is based on the virial theorem and the Faber-Jackson relation, $L \propto \sigma^4$ (Faber & Jackson 1976), which results in the following scaling:

$$R \propto M^{1/2}. \tag{1}$$

and $\rho \propto M^{-1/2}$. The concentration parameter is invariant under any fundamental plane scaling also assuming the Faber-Jackson relation. Therefore all three King model parameters, mass, tidal or maximum radius, and concentration, are fixed for each secondary of given mass. The second is based on recent observed fundamental plane relations (e.g. Pahre et al. 1995, Faber 1995):

$$R \propto M^{0.9}. \tag{2}$$

To reduce the overall number of parameters in this study, I have chosen to retain the Faber-Jackson relation and constant-concentration models, even though recent fundamental relations predict that central density and therefore concentration class scales with mass. Changes in concentration predominantly change the inner profile and, as noted, only weakly effect the overall evolutionary track of the accreted secondary.

There are three remaining parameters: orbital energy, orbital eccentricity and secondary to primary mass ratio. Orbital evolution is determined using local dynamical friction which requires the secondary to be inside the primary (see §3.4). The initial orbits for the secondaries, then, are chosen to have an energy whose circular orbit encloses the 99% of the primary mass. In other words, we consider evolution just subsequent to capture. Eccentricity is parameterized by the ratio of orbital angular momentum to the maximum defined by the energy of the orbit, $\kappa \equiv J/J_{max}(E)$ and five values are chosen: 0.1(0.2)0.9. A pure circular (radial) orbit has $\kappa = 1.0$ ($\kappa = 0.0$). Because a captured elliptical is likely to

[2]The concentration parameter is defined as $\log c \equiv \log_{10}(R_{max}/R_{core})$.

be on a eccentric orbit, we will emphasize the $\kappa = 0.1$ case. The model profile and location of initial orbits in the model is shown in Figure 1. Finally, each set of 5 orbits is evolved for 4 different secondary to primary mass ratios: 10^{-4}, 10^{-3}, 10^{-2}, and 10^{-1}.

Dimensionless units are chosen for the King model such that $G = M = 1$ and total gravitational potential energy $W = -1/2$. For the $W_0 = 9.5$ King model, $R_{core} = 0.5$ with outer radius $R_{max} = 7.91$ in these units. I will take a fiducial central cluster galaxy to have $M = 10^{14}\,\mathrm{M}_\odot$ inside of $R_{max} = 300\,\mathrm{kpc}$ and which sets the time scale quoted in years in §4. This fiducial choice is similar to that for M87 (e.g. Binney & Tremaine 1987, Merritt & Tremblay 1993). A different choice simply shifts the quoted time scale by the ratio

$$\frac{T}{T_o} = \left(\frac{M}{10^{14}\,\mathrm{M}_\odot}\right)^{-1/2} \left(\frac{R_{max}}{300\,\mathrm{kpc}}\right)^{3/2} . \tag{3}$$

For reference, orbital periods for the fiducial scaling whose guiding center radii enclose 10(20)90% for $\kappa = 0.1(0.2)0.9$ are described in Figure 2.

3. Method overview

Evolution in the cannibalized ellipticals is caused by the following four interacting physical effects: 1) resonant heating and orbit shocking; 2) self-consistent gravity; 3) tidal stripping; and 4) dynamical friction. These will be briefly described below and in the Appendix. We will see that dependencies in the effect of the four physical processes govern the subsequent evolution.

3.1. Resonant heating

The orbiting secondary galaxy experiences a differential or *tidal* force. The combined strain and compressive force is time-dependent and can do work on the secondary galaxy. If the change in tidal force is rapid compared to internal orbital time scales, a *gravitational shock*, the work can be computed using the impulse approximation. However even if the change in strain is slower than internal orbital time scales, significant work may still be done: most realistic galaxies will have resonances between the two (or more) internal orbital frequencies the external forcing frequency which leads to significant energy and angular momentum exchange (W1–3).

More picturesquely, the time-dependent force will excite a wake in the secondary. The wake will be dominated by a quadrupole or bar-like distortion whose pattern speed is

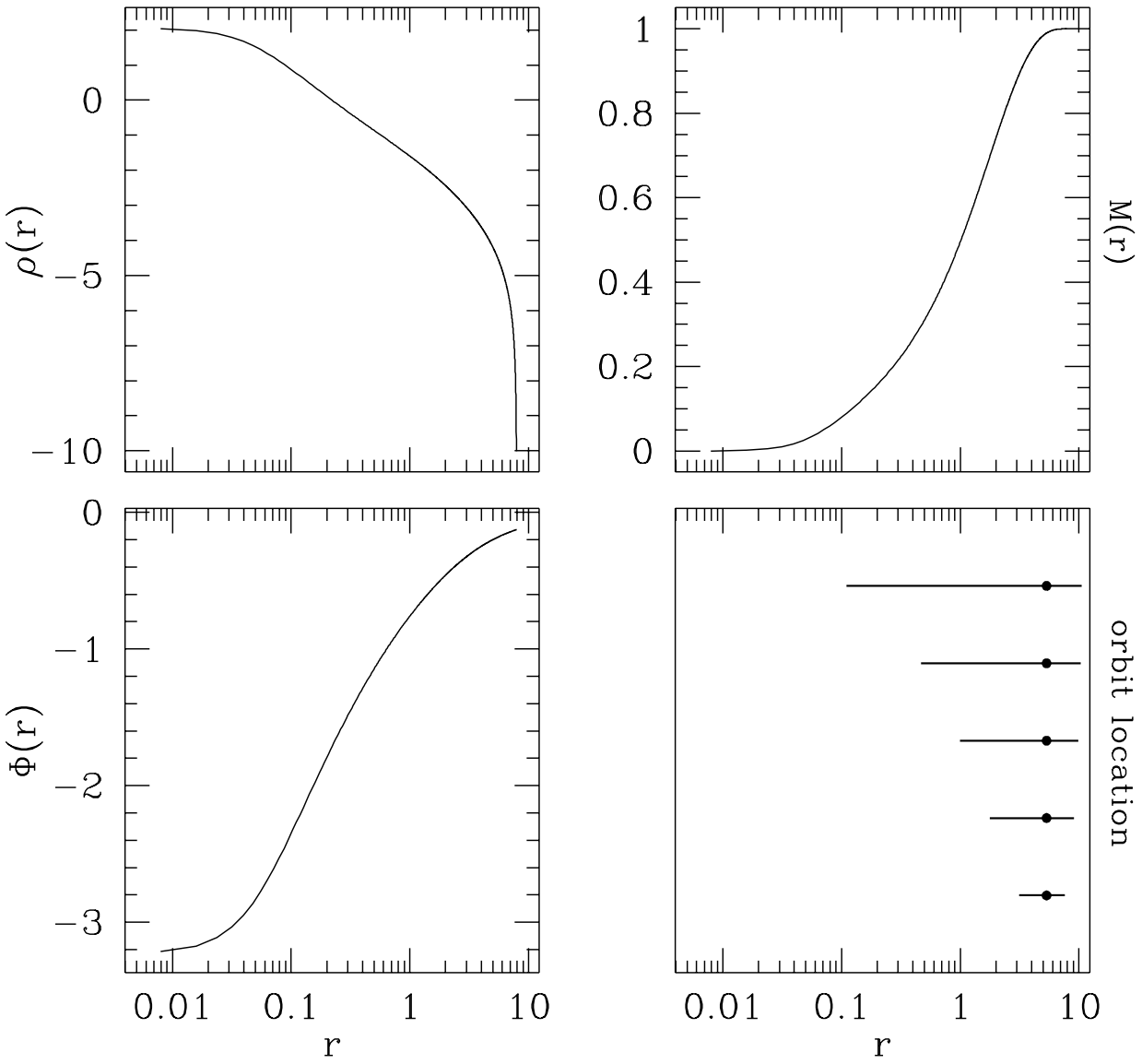

Fig. 1.— Density, mass and potential for $W_0 = 9.5$ King model in dimensionless units. The model is nearly isothermal for $0.05 \lesssim r \lesssim 5$. The diagram at the lower right shows the pericenter and apocenter radii for each orbit (ends of segments) and guiding center (circular orbit) radii (solid dots).

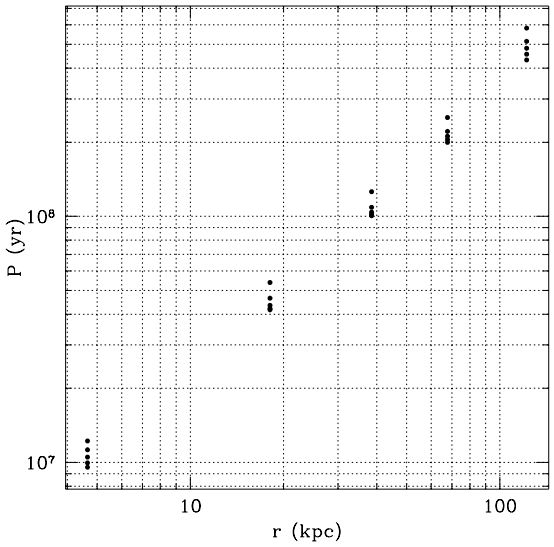

Fig. 2.— Periods of orbit scaled to a central cluster galaxy with $M = 10^{14}\,\mathrm{M}_\odot$ and $R_{max} = 300\,\mathrm{kpc}$. Dots represent the orbital periods with the guiding center radius enclosing 10(20)90% of the primary mass. The values $\kappa = 0.1(0.2)0.9$ are ordered from bottom to top.

determined by the external frequency. Similar to torquing by spiral arms, this 'bar' then couples to the tidal force, transferring energy and angular momentum to resonant orbits. The perturbation-theory-derived heating rates used here are in good agreement with n-body simulations (cf. MW2, Johnston et al. 1996) with the advantage of being able to follow a weak disturbance without noise.

3.2. Self-consistent gravity

By Jeans' theorem (e.g. Binney & Tremaine 1987), an equilibrium of regular orbits is described by a phase-space distribution function, $f = f(\mathbf{I})$ where $\mathbf{I}$ are the actions (or energy and angular momentum for a spherical system). The associated potential and density solve the Poisson equation by construction. Although the actions of most orbits are invariant to the slowly changing tidal strain, the resonant heating described above changes the actions of some small subset of orbits resulting in a slightly out of equilibrium system.

At regular intervals, the Poisson equation is iteratively solved to maintain equilibrium. Because the external force is assumed to do negligible work on an internal orbital time

scale, all external perturbations may be temporarily turned off which fixes the actions and simplifies solution. So the overal evolution consists of two phases: 1) evolution of phase space due to external perturbations in a fixed gravitational potential; and 2) dynamical readjustment with all perturbations removed. Practically, a new equilibrium is only computed when the changing phase-space distribution implies a 1–2% change to the stellar orbits.

As the equilibrium profile evolves, new orbits become resonant with the external force. In this way, a small set of resonant orbits at any one time can change the global structure over a number of dynamical time scales. Finally for the results below, the resulting equilibrium phase-space distribution is forced to be spherical and isotropic. This is not an in-principle demand—the numerical implementation is general—but a choice driven by available CPU time.

3.3. Tidal stripping

The outer boundary of a secondary is defined by the points at which a star is more strongly attracted by the primary. For a circular orbit, this point is the analogous inner Lagrange point in the restricted three-body problem. However, for an eccentric orbit, this is not an easily parameterized problem; these points change as the secondary orbits resulting in foliated stable and unstable regions (e.g. Keenan 1981). N-body simulations suggest that setting the boundary to the inner Lagrange point at perigalacticon is a fair prescription.

The location of the inner Lagrange point scales with the ratio of mean density of the secondary to mean density of the primary enclosed with the secondary's orbit. Therefore, as the secondary evolves due to time-dependent heating as described in §3.1, stars may find themselves on the unbound side of the tidal limit. This loss of material also changes the equilibrium. If too much material is evaporated, global equilibrium may be lost and the smaller galaxy "disrupts".

3.4. Dynamical friction

Finally, the orbit itself is evolving by dynamical friction. For small secondaries, Chandrasekhar's dynamical friction formula is an acceptable approximation (Chandrasekhar 1943, see e.g. Binney and Tremaine 1987). This approximation assumes that the primary is infinite and homogeneous with the local value of density and distribution of velocities. The drag force is anti-parallel to the motion of the secondary assuming velocity isotropy. For

large secondaries, the situation is more complex (e.g. Hernquist & Weinberg 1989, Weinberg 1989) but the local approximation will be used for simplicity. Because the evolution of large secondaries is rapid, it is unlikely that this assumption affects any conclusion. Further consequences of the decaying orbit are an increasing resonant heating rate and stronger tidal limit, both of which accelerate the evolution.

4. Evolution of satellite galaxies

The models and methods of §2 and §3 are applied to groups of twenty models each. Each group of twenty has four mass ratios, $M_{ratio} = 10^{-1}, 10^{-2}, 10^{-3}, 10^{-4}$ and five eccentricities, $\kappa = 0.1(0.2)0.9$ (cf. Fig. 1). The two groups discussed here have guiding center orbits which enclose 99% of the primary mass. The first group uses the virial scaling and the second uses the observed fundamental plane scaling (cf. §2).

Recall that the physical times quoted below assume a primary mass of $10^{14}\,\mathrm{M}_\odot$ inside of 300 kpc. Equation (3) may be used to scale to any desired primary mass and radius.

4.1. Disruption and Survival

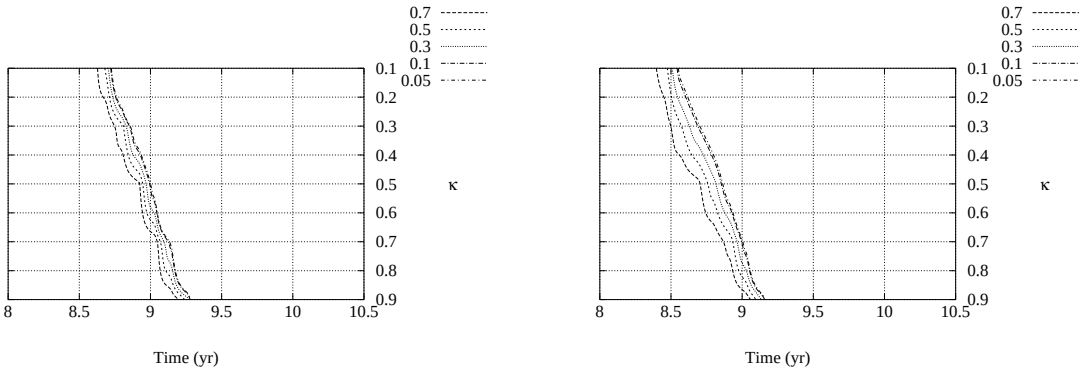

Fig. 3.— Contours show remaining mass fraction (key at upper left) as a function of time (logarithmic scale) and initial value of $\kappa = J/J_{max}$. The secondary to primary mass ratio is 10^{-1}. The right hand (left hand) plot shows the virial (observed) fundamental plane scaling. The scalloping in the contours is caused by the projection of a finite grid.

Figures 3–6 describe the mass evolution for fundamental plane ellipticals as a

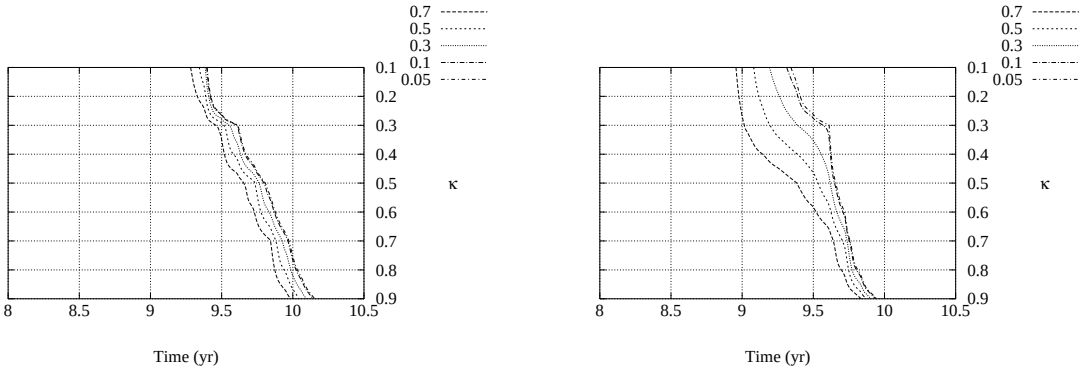

Fig. 4.— As in Fig. 3 but for mass ratio 10^{-2}.

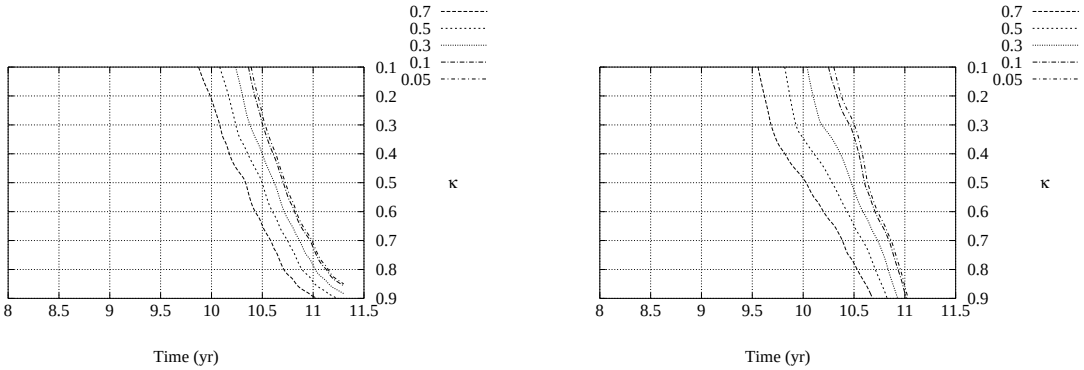

Fig. 5.— As in Fig. 3 but for mass ratio 10^{-3}. Range in time is extended to accommodate alternative scalings.

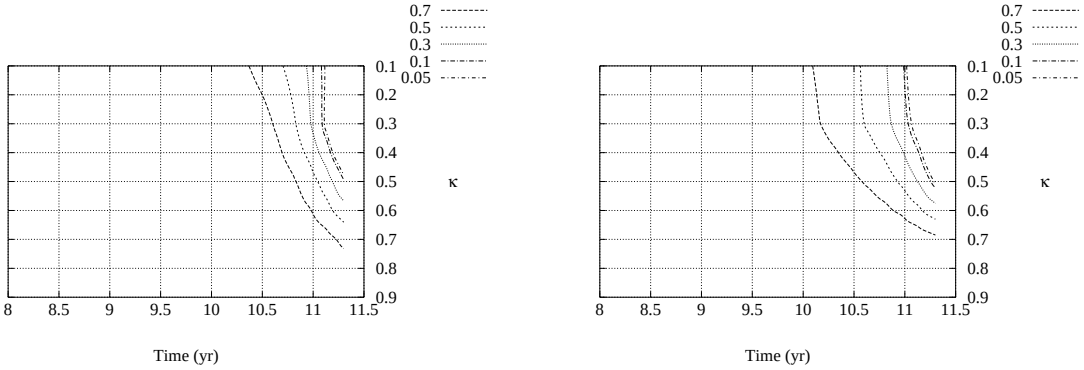

Fig. 6.— As in Fig. 3 but for mass ratio 10^{-4}. Range in time is extended to accommodate alternative scalings.

function of initial eccentricity for the four mass ratios. The contours indicate the mass fraction remaining at the time indicated. The vertical axis shows increasing initial orbital eccentricity. Galaxies to the right of the 0.05 contour have completely evaporated. Heating and stripping is severe for the most eccentric orbits and the highest mass ratios. For the ratio 10^{-1}, the orbit decays quickly and has evaporated for all eccentricities by roughly 1 Gyr (Fig. 3). We will see in §4.2 that disruption occurs near the center of the host galaxy.

The trends are similar for smaller mass ratios. A 1% secondary (Fig. 4) evaporates in 10 Gyr for a nearly circular orbits and in roughly 2 Gyr for an eccentric orbit. A 0.1% secondary—a large dwarf galaxy—does not completely evaporate in 10 Gyr even for an eccentric orbit, although it is close. Evolution is slower for smaller mass ratios because 1) the density of the secondary is larger and therefore couples more weakly to the tidal field; and 2) the orbital decay rate, which is proportional to the mass ratio, is slower.

4.2. Orbital decay

Figure 7 shows the orbital evolution of initially $\kappa = 0.1$ orbits for the four mass ratios. The decay rate is computed using Chandrasekhar's formula with $\ln \Lambda = \ln(R_{max}/r_{1/2})$ where $r_{1/2}$ is the current half-mass radius of the secondary. Orbital torques are also computed in the local approximation with Chandrasekhar's formula. These eccentric orbits becomes more circular during its decay (Fig. 8) as previously described by Bontekoe & van Albada (1987). Initially, the $\kappa = 0.1$ orbits with guiding center trajectories enclosing 99% of the primary mass have apocenters outside the primary (cf. Fig. 1) which may lead to an overestimate of the decay time. For the fiducial model ($M = 10^{14}\,\mathrm{M}_\odot, R_{max} = 300\,\mathrm{kpc}$), only the 10% and 1% mass ratio secondaries can decay into the center in roughly 10 Gyr. The decay time for lower mass galaxies is increased by the concurrent mass loss.

The longer lifetimes for large initial κ is correlated with the longer orbital decay times. This is shown in Figure 9 which describes the evolution of 1% secondaries for $\kappa = 0.3(0.2)0.9$ (the second panel in Fig. 7 is the first member of this sequence with $\kappa = 0.1$). The decay rate is nearly constant for orbits in the inner primary (roughly inside the half-mass radius of 60 kpc). The rate increases with decreasing initial eccentricity because the secondary spends a larger fraction of its time at higher primary density. This trend decreases the spread of decay times with eccentricity, but does not compensate for the slower initial evolution of low-eccentricity orbits.

Similarly, the steep gradient in time across the mass contours in Figures 3–6 reflects the rapid mass evolution which takes place during the final stage of orbital decay. This

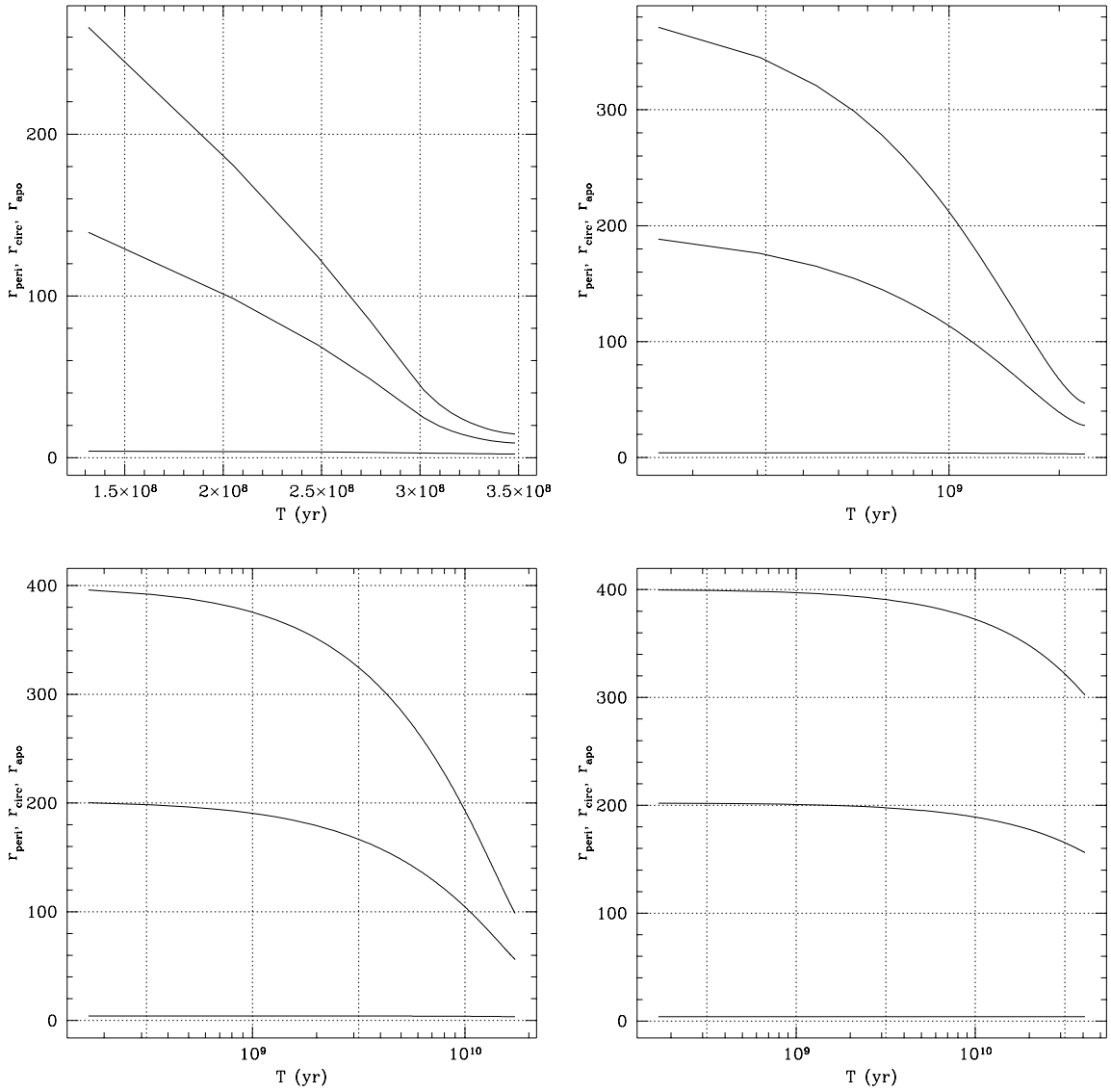

Fig. 7.— Orbital evolution for initial $\kappa = 0.1$ orbits for the four mass ratios $10^{-1}, 10^{-2}, 10^{-3}, 10^{-4}$ (right to left, top to bottom) with observed fundamental plane scaling (cf. Figs. 3—6). Satellites with $M_{ratio} = 10^{-1}$ and 10^{-2} have zero mass at the final time shown.

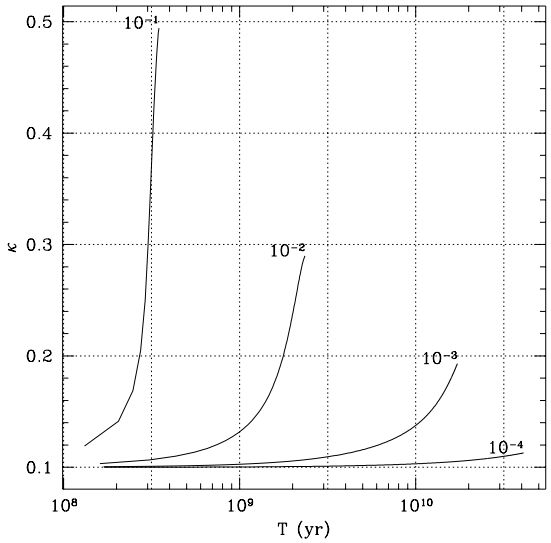

Fig. 8.— Change in $\kappa = J/J_{max}$ for mass ratios indicated for orbits with $\kappa = 0.1$ initially.

trend is maintained at the smallest mass ratios although full decay takes longer than a galaxian age for the fiducial scaling.

Combining the results of this and the previous subsection, we reach the conclusion that *satellites which can fall to the center of a cluster giant by dynamical friction are evaporated by internal heating.*

4.3. Distribution of stripped material

As the secondary is stripped and disrupted, its stars preserve the instantaneous orbit and build up the primary as suggested by Richstone (1976). The relative density distributions for secondaries on eccentric orbits, $\kappa = 0.1$, and the four mass ratios are shown in Figure 10.

The higher-mass secondaries, $M_{ratio} = 10^{-1}$ and 10^{-2}, lose mass quickly. Material is lost most quickly at pericenter and individual episodes of mass loss during each orbit are visible in the outer galaxy. For $M_{ratio} = 10^{-1}$, 90% of the mass is lost within the half-mass radius of the primary and 20% within 4 core radii. Overall, the remnant profile is steeper than the primary and could be a significant contributor to the inner light after a few such events. The two low mass ratio cases, $M_{ratio} = 10^{-3}$ and 10^{-4}, lose mass more

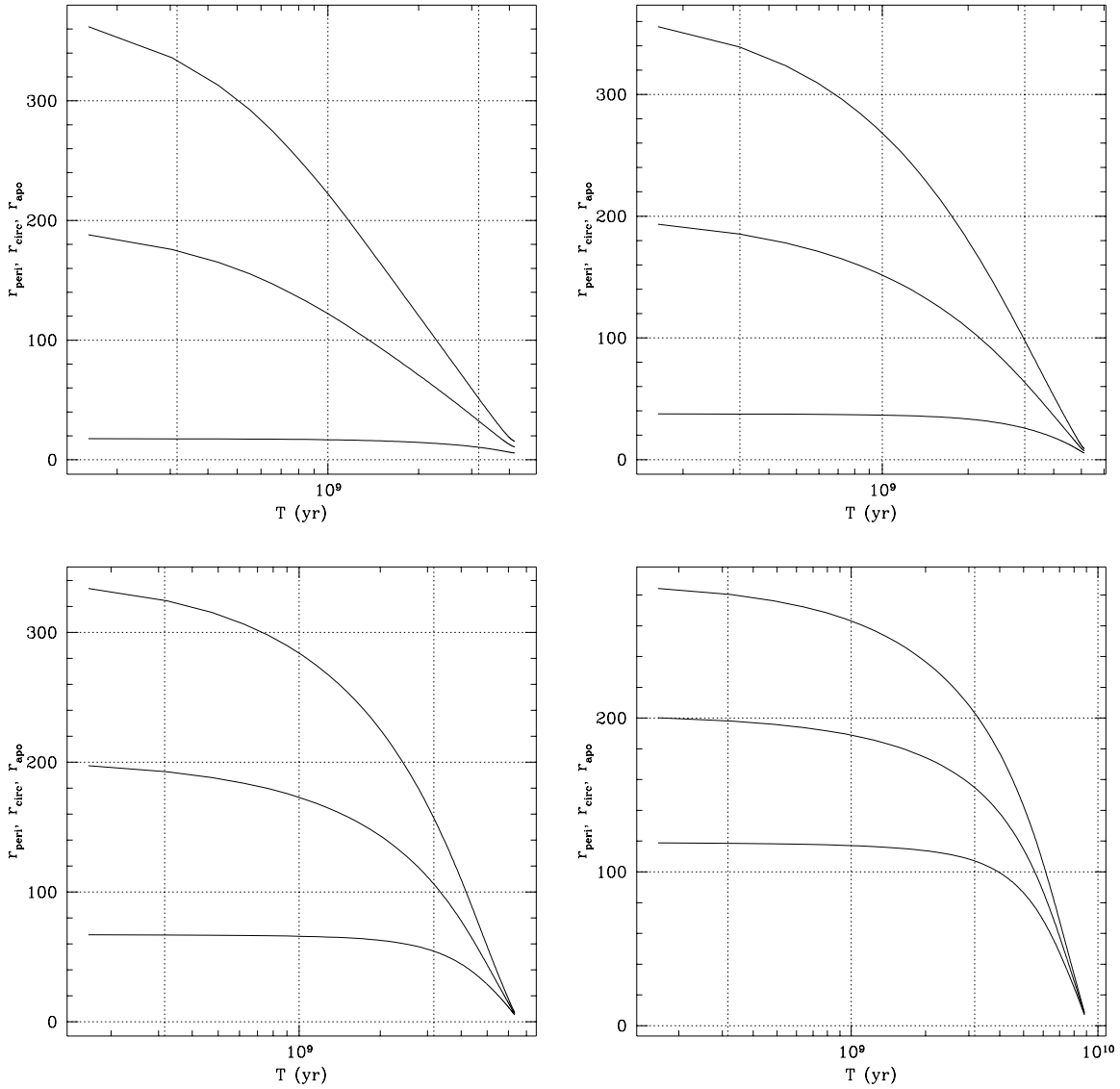

Fig. 9.— Orbital evolution for initial $\kappa = 0.3, 0.5, 0.7, 0.9$ orbits for mass ratios 10^{-2}, with observed fundamental plane scaling.

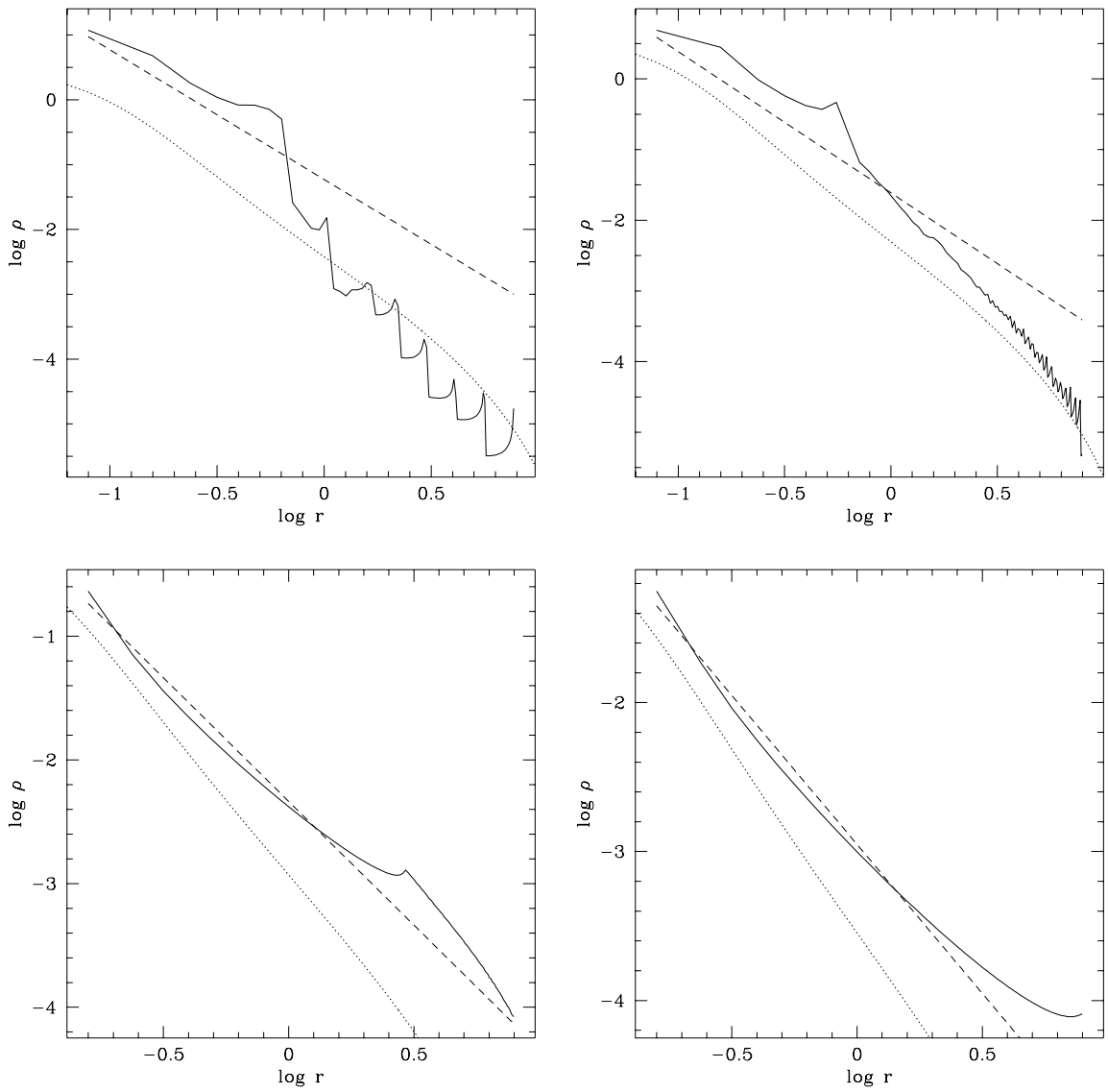

Fig. 10.— Distribution of stripped material from disrupting secondary (solid curve) compared with r^{-2} profile (dashed) and background density (dotted) at the four mass ratios $10^{-1}, 10^{-2}, 10^{-3}, 10^{-4}$ (right to left, top to bottom). These use the virial scaling and dimensionless units (§2.1).

gradually and the distribution of stars lost in the outer primary is more extended than the primary, approximating a r^{-2} distribution. Both have guiding center radii larger the primary half-mass radius and have lost roughly 80% and 50% of their total mass at the point depicted.

Overall, these results suggest that *mass evaporated from the secondary is distributed similarly to and maybe steeper than the profile of the primary.* After many accretion events, the merged profile will be slightly more concentrated (c.f. Fig. 10).

4.4. Comparision with previous n-body simulation

Unfortunately, there has been very little reported n-body work on merging for self-consistent primary and secondary galaxies with masses differing by orders of magnitude. A search of the literature (Quinlan 1996/nociteQuin:96) revealed one similar n-body study by Balcells & Quinn (1990) who performed simulations with $M_{ratio} = 0.1, 0.2$ for rotating systems to explore the formation of counterrotating cores. Although the their initial conditions and goals are sufficiently different to prevent a precise comparison, the results here yield a similar scenario. The orbital decay is rapid with the largest fraction the secondary evaporating in or near the core (c.f. Fig. 3 and the first panel of Figs. 7 and 10.). Although Balcells & Quinn conclude that the dense core of the smaller galaxy *survives* the orbital decay and settles in the core, I believe that we describe the same the end result: a single merged profile rather than a multiple nucleus system. Clearly, this is subject is ripe for additional work.

5. Summary and discussion

The major conclusions of this work are as follows:

- Time-dependent heating will evaporate secondaries with mass ratios as small as 1% on *any* initial orbit well within a galaxian age. The difference with the naive prediction that the denser satellite galaxies will invariably survive orbital decay is due to the breakdown of the one-dimensional adiabatic invariant in three-dimensional stellar systems as described in MW1.

- Secondaries with mass ratios as small as 0.1% on eccentric orbits are significantly evolved and nearly evaporated. Because capture by dynamical drag will preferentially produce high-eccentricity companions, this predicts a lower limit: *captured secondaries*

with mass smaller than 0.1% of the primary will not evaporate.

- Captured satellites with mass ratios smaller than roughly 1% will not decay to the center in a galaxian age. This limit may be conservative—even lower mass secondaries will decay to the center and evaporate—given evidence gravitational lens results (Miralda-Escudé 1995) that the optically inferred mass profile of cD galaxies joins smoothing on the that of the cluster in general.

- The profile of the mass lost as the satellite decays is similar to but slightly more concentrated than that of the original primary. This implies that that the concentration of the cluster giant will gradually increase after many mergers.

- Altogether, we have the result that satellites which can fall to the center of a cluster giant by dynamical friction are evaporated by tidal heating in the process. Disruption occurs near the center of the primary; material from both cores combine into a single entity. This suggests that true multiple nuclei giants should be rare. This scenario does not address the possibility that a massive accretion event will lead to a nuclear gas accretion and a burst of star formation (Hernquist & Mihos 1995) and perhaps form a second nucleus in situ.

I thank Sandy Faber, Gerry Quinlan, Chigurupati Murali, Doug Richstone and Scott Tremaine for comments and suggestions. This work was supported in part by NASA grant NAGW-2224, NAG 5-2873 and the Sloan Foundation.

REFERENCES

Binney, J. and Tremaine, S. 1987, *Galactic Dynamics*, Princeton University Press, Princeton.

Bontekoe, T. R. and van Albada, T. S. 1987, MNRAS, 224, 349.

Chandrasekhar, S. 1943, ApJ, 97, 255.

Chang, J. S. and Cooper, G. 1970, J. Comp. Phys., 6, 1.

Faber, S. M. 1995, *private communication.*

Faber, S. M. and Jackson, R. E. 1976, ApJ, 204, 668.

Hernquist, L. and Mihos, C. J. 1995, ApJ, 448, 41.

Hernquist, L. and Weinberg, M. D. 1989, MNRAS, 238, 407.

Johnston, K. V., Hernquist, L., and Weinberg, M. D. 1996, *Tidal effects on spherical stellar systems*, in preparation.

Keenan, D. W. 1981, A&A, 95, 334.

Lauer, T. R. 1988, ApJ, 325, 49.

Merritt, D. and Tremblay, B. 1993, AJ, 106, 2229.

Miralda-Escudé, J. 1995, ApJ, 438, 514.

Murali, C. and Weinberg, M. D. 1996a, *The Effect of the Galactic Spheroid on Globular Cluster Evolution*, submitted to *Monthly Notices*, archived at `http://babbage.sissa.it` (MW1).

Murali, C. and Weinberg, M. D. 1996b, *Globular cluster evolution in M87*, submitted to *Monthly Notices*, archived at `http://babbage.sissa.it` (MW2).

Pahre, M. A., Djorgovski, S. G., and de Carvalho, R. R. 1995, ApJ, 453, L17.

Richstone, D. O. 1976, ApJ, 204, 642.

Tonry, J. L. 1985, AJ, 90, 2431.

Tremaine, S. 1995, *private communication*.

Vader, J. P. and Chaboyer, B. 1994, AJ, 108, 1209.

Weinberg, M. D. 1989, MNRAS, 239, 549.

Weinberg, M. D. 1994a, AJ, 108, 1398 (W1).

Weinberg, M. D. 1994b, AJ, 108, 1403 (W2).

Weinberg, M. D. 1994c, AJ, 108, 1414 (W3).

A. Orbit shocking

Shocking caused by an oscillatory perturbation is a straightforward variant and is somewhat easier to compute than a one-shot adiabatic disturbance described in W2. For example, if a cluster is dynamically part of the thick disk, then the perturbation has the form $V_p = g(t)z^2$ where then $g(t)$ is a periodic function of time. The function $g(t)$ may be expanded as a Fourier series in its vertical oscillation period, P:

$$g(t) = \sum_{k=-\infty}^{\infty} g_k e^{ik\omega t}, \tag{A1}$$

where $\omega = 2\pi/P$ and

$$g_k = \frac{1}{P}\int_0^P dt\, g(t) e^{-ik\omega t}. \tag{A2}$$

The Laplace transform of this Fourier series is trivial and is:

$$\hat{g} = \sum_{k=-\infty}^{\infty} \frac{g_k}{s - ik\omega}. \tag{A3}$$

For physical scenarios (e.g. smooth and continuous mass profiles), g_k will converge rapidly with increasing $|k|$. The calculation is analogous for orbit shocking with the following changes:

1. The potential perturbation expansion will be more general than the $\propto z^2$ dependence and include all 2nd order moments (all Y_{2m} terms);
2. The Fourier expansion of $g(t)$ will have two indices corresponding to the radial and azimuthal periods of the cluster orbit.

See MW2 for details.

We are only interested in the long-term secular change in the distribution function, after any transients have decayed. Following W2, we Fourier-Laplace transform the perturbed Boltzmann equation. The secular contribution is second-order distribution function and the inverse Laplace transform leads to the desired result. The details of the function $g(t)$ are not important which allows one to eliminate it altogether (MW2). Alternatively, one can choose a convenient form for $g(t)$, such as a square pulse, and perform the transforms explicitly. Either way for time scales large compared to the stellar orbital times, the secular change due to heating becomes

$$\frac{d\, f_2}{dt} = \pi \sum_{k,\mathbf{l}} |g_k|^2\, \mathbf{l}\cdot\frac{\partial}{\partial \mathbf{I}}\left(V_{t\,\mathbf{l}} V_{t\,-\mathbf{l}}\right)\, \mathbf{l}\cdot\frac{\partial f_o}{\partial \mathbf{I}}\delta\left(k\omega + \mathbf{l}\cdot\mathbf{\Omega}\right)$$

where $V_{t\mathbf{l}}$ denotes the action-angle transform of the tidal potential. As described in MW2, this expression has the form:

$$\frac{\partial f}{\partial t} = \frac{d\, f_2}{dt} = \frac{\partial}{\partial E}\left\{ A(E) \frac{\partial f}{\partial E} \right\} \tag{A4}$$

which may be solved by standard techniques (e.g. Crank-Nicholson or Chang-Cooper 1970 schemes).

MW3 will describe the effects disk-shocking, orbit shocking and thick-disk shocking on the galactic population of globular clusters.

B. Tidal perturbation

To compute the effect of an orbit in a galaxy, the Galactic potential may be expanded in the cluster frame. The force (inertial) is:

$$\mathbf{F}_t = -\nabla\Phi|_{\mathbf{R}+\mathbf{r}} + \nabla\Phi|_{\mathbf{R}} \tag{B1}$$

$$F_i \approx -\sum_j \left.\frac{\partial^2\Phi}{\partial x_i \partial x_j}\right|_{R=R(t)} x_j, \tag{B2}$$

where $\mathbf{R}$ describes the cluster and $\mathbf{r}$ the position of a star relative to the cluster. The tidal potential then follows directly:

$$V_t = \frac{1}{2}\left\{ \left(\frac{d^2\Phi}{dR^2} - \frac{1}{R}\frac{d\Phi}{dR} \right) \frac{(\mathbf{R}\cdot\mathbf{x})^2}{R^2} + \frac{1}{R}\frac{d\Phi}{dR}\, r^2 \right\}\Bigg|_{\mathbf{R}=\mathbf{R}(\mathbf{t})}. \tag{B3}$$

Expanding equation (B3) in spherical harmonics, perturbed quantities may be computed as outlined in §A. The non-inertial velocity-dependent forces are not easily incorporated into a potential and have been ignored here.